Differential elastic electron scattering by pentane

Kamil Fedus, C. Navarro, L. R. Hargreaves, M. A. Khakoo, Alessandra Souza Barbosa, and M. H. F. Bettega

Phys. Rev. A **91**, 042701 — Published 1 April 2015

DOI: 10.1103/PhysRevA.91.042701

DIFFERENTIAL ELASTIC ELECTRON SCATTERING BY PENTANE

Kamil Fedus,
Institute of Physics, Faculty of Physics, Astronomy and Informatics, Nicolaus Copernicus University, Grudziadzka 5, 87-100 Torun, Poland, EU,

C. Navarro, L. R. Hargreaves and M. A. Khakoo,
Department of Physics, California State University, Fullerton, California 92834

and

Alessandra Souza Barbosa and M. H. F. Bettega,
Departamento de Física, Universidade Federal do Paraná, Caixa Postal 19044, 81531-990 Curitiba, Paraná, Brazil

(Dated: January 29 2015)

Abstract: We report measurements and calculations of the differential cross sections for elastic scattering of low-energy electrons by pentane, C_5H_{12}. The incident energies measured are at 1, 1.5, 2, 3, 5, 10, 15, 20, 30, 50, 100eV, and the calculations covered energies up to 100 eV. The range of experimental scattering angles is from 5^o to 130^o. We compare our experimental and theoretical values to each other and to available experimental and theoretical data for linear n-alkanes.

PACS numbers: 34.80Uv, 34.80.Bm

1. Introduction.

Next to the molecule n-butane (nC_4H_{10}, with a research octane number of 94), n-pentane (nC_5H_{12}, with a research octane number of 62) is the simplest liquid hydrocarbon (at room temperature) contained in gasoline engines and is a major constituent of liquefied petroleum gas (LPG), an important alternative fuel for automobiles [1, 2]. Ignition and reaction chemistry involving excitation, dissociation and ionization of these molecules in combustion (plasma) processes in automobile engines [3] are governed/catalyzed by energetic electron scattering from these fuel species in the energy region which ranges from 0.1eV to high energies (>100eV), but with a maximum around 10eV [4]. Whereas there exist electron impact data on methane [5,6,7], ethane [8,9], propane [10,11,12] and butane [13] and references cited within these, there is lack of electron collision data for pentane. The few data available for pentane are those by Freeman *et al.* [14] of total electron cross sections determined from the mobility of electrons in liquid pentane at the energies of 0.1 to 0.5 eV using a time-of-flight method and those by Kimura *et al.* [15] of gaseous pentane of total cross sections for this target. Floriano *et al.* [16] also reported momentum-transfer cross sections (MTCS) for gaseous pentane in the region of Ramsauer-Townsend (RT) minimum from swarm-type experiments.

Electron scattering studies of larger polyatomic molecules have received impetus since the discovery by Boudaïffa *et al.* [17], that low energy secondary electrons were able to dissociated DNA molecules via dissociative electron attachment (DEA), which is a resonant process. This has important biological implications concerning electron impact processes on organic molecules. Whereas much work has been carried out on those molecules that make up the DNA bases or its backbone sugar, significantly less work, of similar nature, is available on the role of electrons on hydrocarbon fuels, especially in the vapor phase (obtained from a room temperature

volatile liquid) which would be used in automotive systems for both regular and diesel engines, and where combustion in engines is initiated by electrons from a spark plug or produced by compression of the gas to high temperatures to produce free electrons. One can expect DEA processes to similarly take place in these environments and to have a significant effect on the efficiency of combustion processes. In this paper we present an effort to cover this gap with pentane which is a liquid at room temperature as compared to propane or butane, which have been investigated in the past.

The present measurements of differential cross sections (DCSs) for elastic electron scattering from pentane were taken at incident electron energies (E_0) of 1eV to 100eV for scattering angles (θ) of 5^o to 130^o using our low-intermediate energy electron spectrometer [18]. Our calculations were carried out using the Schwinger multichannel (SMC) method [19,20] with pseudopotentials [21] and were carried out in the static-exchange (SE) and static-exchange plus polarization (SEP) approximations. In addition, we compare our DCSs with similar SEP calculations for n-pentanol, $C_5H_{11}OH$, which is close in structure to pentane, but has a significantly larger dipole moment. At energies significantly above the ionization potential of pentane at 10.37eV [22], we employ the SMC with just in the SE approximation. A ball-and-stick model of pentane is shown in Fig. 1 which illustrates its chain-like structure and gives the positioning of C-C bonds and C-H bonds and shows how its dipole moment would be small.

The remainder of this manuscript is as follows. In Sec. 2.1 we present our experimental procedures and on Sec. 2.2 our theoretical method and the computational procedures employed in the present calculations. Our results and discussions are presented in Sec. 3. We end the paper with a short conclusion about our findings.

2. Method.

2.1. Experimental

Our experimental apparatus, which has been well-tested, is detailed in our previous papers, e.g. Khakoo *et al.* [18], so only a short a summary of it is given here. The electron gun and electron analyzer had double hemispherical energy selectors to provide well-defined electron beam energy profiles. The apparatus was made of titanium cylindrical lenses with molybdenum apertures. The system was baked at a temperature of about 130^{o}C using biaxial heaters [23] which did not add any significant magnetic field to our system when operated. Electrons were detected by a discrete dynode electron multiplier [24], which had a dark count rate of <0.01Hz and which was capable of linearly detecting >10^5 Hz of electrons without saturating. The remnant magnetic field in the collision region area was reduced to ≈1mG at the collision region by a double μ-metal shield, coupled with a Helmholtz coil that eliminated the vertical component of the Earth's magnetic field. Typical electron currents ranged around 18-28 nA, with a corresponding energy resolution of between 40-50meV, full-width at half-maximum. Lower currents were chosen for lower E_0 values in order to curtail the effects of space-charge broadening of the incident electron beam, whereas higher currents were employed at our higher energies to obtain better statistics at larger scattering angles. The electron beam varied less than 10% at maximum during the day's data acquisition. The energy of the beam was established by, at least daily, measuring the minimum in elastic scattering of the 2^2S He- resonance at E_0=19.366eV [25] at θ=90^{o} to better than ≈30meV stability during an experimental run (1 day). Typically the contact potential varied from 0.6 eV to 0.7 eV. Energy loss spectra of the elastic peak were collected at fixed E_0 values and θ by repetitive, multi-channel-scaling techniques. The effusive target gas beam was formed by flowing gas through a ≈0.3mm diameter aperture mounted at the end of a ¼" aluminum tube. The whole source was sooted (using

an acetylene flame) to reduce secondary electrons. The use of an aperture instead of a tube gas collimator, removes the need to maintain the gas pressures of the target gases in an inverse ratio of their molecular diameters, removing a major systematic source of error that occurs in using tube collimators or similar, see e.g. [26]. The aperture source was located ≈5mm below the axis of the electron beam, and the source was moveable in and out of alignment with electron beam. This moveable gas source arrangement [27] enabled us to expediently and accurately determine background electron-gas scattering rates. The measured DCSs were normalized using the well-known Relative Flow Method with helium as the reference gas, using DCSs from the well-established work of Nesbet [28] for E_0 < 20eV and of Register *et al.* [29] for E_0 ≥ 20eV. The pressures behind the aperture ranged from 1.2 to 2.5 torr for He and 0.065 to 0.1 torr for pentane, resulting in a chamber pressure ranging from 1.0×10^{-6} torr to 2×10^{-6} torr. Each DCS was taken a minimum of two times to check its reproducibility and a weighted average was made of multiple data sets to obtain the final DCSs. Integral cross sections (ICS) and MTCS were evaluated from the measured DCS by extrapolating the DCS to zero and 180 degrees and applying the standard integral formula. Each DCS set was extrapolated to $\theta=0^o$ and 180^o by a polynomial curve which is described in [30].

2.2. Theory and Computational Details.

Our calculations were carried out using the SMC method with pseudopotentials (SMCPP) [21]. The details of the method are not the main purpose of this work, and we will provide only the relevant points for the present calculations. The SMC method is a variational approximation to the scattering amplitude, $f_{SMC}(\vec{k}_f, \vec{k}_i)$, with $\vec{k}_f, \vec{k}_i$ being the incident and scattered electron momenta. The expression for the scattering amplitude in the body-frame is given by:

$$f_{SMC}(\vec{k}_f,\vec{k}_i)=\frac{1}{2\pi}\sum_{m,n}\left\langle S_{\vec{k}_f}\middle|V\middle|\chi_m\right\rangle\left(d^{-1}\right)_{mn}\left\langle\chi_m\middle|V\middle|S_{\vec{k}_i}\right\rangle \quad , \qquad (1)$$

where the $\{|\chi_m\rangle\}$ represents a basis set of (N+1) – electron symmetry-adapted Slater determinants, also referred to as configuration state functions (CSFs). The CSFs are built from products of target states with one-particle wave functions. For the calculations carried out in the static-exchange (SE) approximation, the (N + 1)-electron basis set (direct space) is given by

$$\left|\chi_m\right\rangle=\mathsf{A}\left(\left|\Phi_1\right\rangle\otimes\left|\phi_m\right\rangle\right) \quad , \qquad (2)$$

where $|\Phi_1\rangle$ is the target ground state, $|\phi_m\rangle$ is a single-particle function and A is the antisymmetrizing operator. For the calculations carried out in the static-exchange plus polarization (SEP) approximation, the direct space is augmented by CSFs constructed as

$$\left|\chi_m\right\rangle=\mathcal{A}\left(\left|\Phi_r\right\rangle\otimes\left|\phi_s\right\rangle\right) \quad , \qquad (3)$$

where $|\Phi_r\rangle$ are N-electron Slater states obtained by performing single excitations of the target from the occupied (hole) orbitals to a set of unoccupied (particle) orbitals. Here $|\phi_s\rangle$ is also a single-particle function.

In Eq. 1, the d_{mn} matrix elements are given by,

$$d_{mn}=\left\langle\chi_m\middle|\mathsf{A}^{(+)}\middle|\chi_n\right\rangle \quad , \qquad (4)$$

and the $\mathsf{A}^{(+)}$ operator is given by,

$$\mathsf{A}^{(+)}=\frac{1}{2}(PV+VP)-VG_P^{(+)}V+\frac{\hat{H}}{N+1}-\frac{1}{2}(\hat{H}P+P\hat{H}) \quad . \qquad (5)$$

In the above equations $S_{\vec{k}_f}$ is a product of a target state and a plane wave with momentum $\vec{k}_{i(f)}$, which is an eigenstate of the unperturbed Hamiltonian H_0; V is the interaction potential between the incident electron and the target; $\hat{H} \equiv E\text{-}H$ is the collision energy minus the full Hamiltonian of

the system, with $H = H_0 + V$; P is a projection operator onto the open-channel space and $G_P^{(+)}$ is the free-particle Green's function projected on the P-space.

Our scattering calculations were carried out in the optimized geometry of pentane, which belongs to the of C_{2v} symmetry group. In order to optimize the pentane ground state geometry we employed the density functional theory (DFT) with the hybrid three-parameter Becke-Lee-Yang-Parr (B3LYP) functional and the DZV++(2*d,p*) basis set, as implemented in the package GAMESS [31]. Figure 1 shows a diagram of the geometrical structure of the molecule.

We used the pseudopotentials of Bachelet *et al.* [32] to replace the core electrons of the carbon atoms and the valence electrons are represented by Cartesian Gaussian functions which were generated according [33]. The Cartesian Gaussian basis set used in the present calculations are given elsewhere [34,35]. For hydrogen, we used the 4s/3s basis set of Dunning [36] augmented by one *p*-type function with exponent 0.75. The symmetric combinations of the *d*-type orbital were excluded to avoid linear dependency in the basis set.

To represent the particle and scattering orbitals we employed modified virtual orbitals (MVOs) [37], which were generated by diagonalizing a cationic Fock operator with charge +6. The SEP space was formed by singlet- and triplet-coupled single-particle excitations from all valence occupied orbitals to the 60 lowest-energy MVOs. We also employed 60 MVOs as scattering orbitals and obtained 14998 CSFs for A_1 symmetry, 14923 CSFs for B_2 symmetry, 13991 CSFs for B_1 symmetry and 13919 CSFs for A_2 symmetry.

3. Results and Discussion.

3.1 Pentane.

The DCSs measured in this work and the ICSs and MTCSs determined from them are presented in Table I. In Fig. 2 we present our calculated integral cross section (ICS), in the SEP approximation, for energies up to 20 eV. We also present in this figure experimental elastic ICS for electron scattering by pentane. We compare our results with experimental total cross section (TCS) from [15] for electron collision with pentane and calculated data for elastic electron collision with n-pentanol obtained with the SEP approximation [38]. The alcohol, n-pentanol, is obtained from pentane by the replacement of a hydrogen in the first carbon by a OH group. One can notice a large difference between pentane and n-pentanol ICS for low energies, due to the permanent dipole moment present in the n-pentanol alcohol (1.63 D), while pentane molecule has a very small (presently calculated) dipole moment (0.08 D). We find good agreement between our calculated data with experimental TCS data [15], mainly in the structure position at 8.5 eV. Agreement between the present experimental elastic ICSs and the TCS of [15] is good below E_0=5eV except that the rapid rise in the ICSs below 2eV is not observed in the TCSs. The disagreement at 10eV between our experimental and calculated ICSs and the TCSs can be understood to be due to the inclusion of inelastic channels. Above 10eV the opening up of inelastic and ionization channels is consequently responsible for the observed differences between the experimental ICSs and TCSs of this SEP approximation and [39].

In order to characterize the theoretical ICS energy dependence, we show in Fig. 3 the symmetry decomposition of the ICS, according to the C_{2v} point group. In particular, the broad structure in the SEP ICS at around E_0=8.5eV presented in Fig. 2, can be explained as due to the overlap of structures belonging to all symmetries and located at around 8 eV in the symmetries A_1 and A_2, and at around 9 eV in the symmetries B_1 and B_2.

In Figs. 4, 5 and 6 we present our calculated differential cross sections (DCSs) at selected energies between 1 and 100 eV. For energies up to 20 eV we present results in the SEP approximation and for higher energies we present results in the SE approximation. We also compare our calculated DCSs with calculated DCS for n-pentanol [38] and with experimental DCSs for pentane. In Fig. 4, at our lowest E_0 values of 1eV and 1.5eV, the experimental DCSs show rapid change in angular behavior from a strongly backward-scattering at E_0=1 eV to a *d*-type angular distribution at E_0=1.5 eV, which is not observed in the SEP results, although this picture improves at E_0=2 eV, showing forward scattering typically due to the static dipole polarizability of pentane which average value is large at $\approx 9.6 Å^3$ [40]. The low energy experimental DCSs clearly demonstrate the role of polarizability of pentane at even our lowest E_0 values. Such rapid changes in DCS angular distributions with E_0 at low E_0 values are typical of such alkane targets and have been seen e.g. in [10,41,42].

For E_0 higher than E_0=2 eV as we see much-improved agreement with our SEP calculations, and increased forward scattering due to the influence of target polarizability. A prominent secondary maximum around $\theta=70^o$ first observed at E_0=1.5 eV persists up to the ionization energy. At E_0=5 eV to 15 eV agreement between experiment and the SEP is very good. We also observe that the SEP values from pentanol follow those of pentane, except that the permanent dipole of pentanol produces a somewhat more pronounced forward peak at E_0=5 eV and 10eV. Above the ionization potential, this is no longer the case and the polarizability is more dominant. We observe an *f*-wave behavior in the theoretical and experimental DCSs around 10 eV. For higher energies, there are some discrepancies in magnitude between the calculated and the experimental DCSs. This is due because our calculations consider only the elastic channel, and there is no flux loss from the elastic channel into the inelastic channels. It has been shown that including the inelastic

channels the DCSs move down toward the experimental data [39,43]. At $E_0 \geq 20$eV intermediate to large θ agreement between the theory (SE/SEP) is much reduced, as is expected, due to the close-coupling breakdown of the theory not to be able to include the increase in the scattering channels greatly above the ionization energy as shown in Figs. 5 and 6.

In Fig. 7 we show the calculated SEP elastic DCSs for E_0 from 5eV to 10eV in 1eV steps illustrating the *f*-wave dependence (with DCS minimum at $\theta=90^o$) in angular distribution around the 8eV resonance energy. A similar behavior is observed in alkanes, alcohols and amines of straight chain structures [30,35,38,44-46]. This is in contrast to branched-chain molecules where the *d*-type behavior is observed (i.e. a DCS local maximum at $\theta=90^o$).

In Fig. 8 we show our $\theta=90^o$ DCSs as a function of E_0 from 0.317eV to 20eV (so-called "excitation curve"). Our experimental 90^o DCSs (taken at fixed E_0 values vs θ, and taken at the fixed $\theta=90^o$ vs E_0) are in good agreement with each other, however we observe a sharp maximum at about 0.37eV (see inset in the figure), due to a Feshbach resonance followed by a broader shape resonance feature at around 8.3eV (due to the symmetry components of Fig. 3) that is observed to be much sharper in the SEP theory than experiment. Both theory and experimental DCSs decrease sharply as E_0 approaches 0eV, where we can expect a RT minimum as expected for alkanes e,g. [Floriano *et al.* 16]) where the minimum is at an E_0 value not possible to access with the present experiment. This type of minimum was also observed in the computed cross sections for alcohols, such as methanol, ethanol, n-propanol, n-butanol and n-pentanol [38].

3.2. Comparison with other linear n-alkanes.

Floriano *et al.* [16] noticed from swarm experiments that the RT minimum in the electron momentum transfer cross section (MTCS) occurs at the same energy (~0.12eV) in all n-alkanes

from C_2H_6 to $C_{10}H_{22}$. Moreover the experiments show [16] that it is the molecular size rather that determines the magnitude of the MTCS rather than the energy dependence. A weak energy dependence on chain length indicates that the electron being scattered interacts with chain segments that contains only two or three carbon atoms. The longer chain mainly increases the number of scattering centers enhancing the average cross section. Here we notice a similar trend for DCS of n-alkanes – the length of molecular chain changes more the magnitude of DCS than the shape of its angular dependence for a given E_0. This general tendency is presented in Fig. 9 where we compare our experimental DCS for pentane (C_5H_{12}) with available DCS experimental data for shorter linear alkanes C_nH_{2n+2} from this family such as ethane (C_2H_6), propane (C_3H_8) and butane (C_4H_{10}). While there are low and intermediate E_0 (< 50 eV) elastic DCSs for ethane and propane, only intermediate E_0 (> 50 eV) DCSs exist for butane [13].

At E_0=2eV and 3eV, the experimental DCS data display similar angular distributions with a forward (polarizability) peaking followed by a minimum at around θ=40-50^o and a maximum around 80^o. At higher energies the shapes are identical except that the ethane and propane DCSs are generally (and expectedly) lower in magnitude than present results for pentane. The very early DCSs of Fink *et al.* [51] likely suffer from normalization effects and are somewhat of different angular behavior as most other DCSs. In particular, the DCS data for propane [10] are lower by a factor of ≈0.76, which roughly reflects the ratio of chain lengths. At E_0=100eV, where we can also compare to butane DCSs we see butane's DCSs range in between pentane and propane, as expected, being lower than pentane by a factor of ≈0.88, allowing for experimental uncertainties. At small θ, our DCSs are lower than some data for other alkanes what we attribute to problems in background evaluation from the other experiments as compared to the present where our moveable source arrangement is expected to produce a better characterization of the background.

4. Conclusion.

We have presented theoretical and experimental differential elastic scattering cross sections for pentane using the Schwinger multichannel method with pseudopotentials and the aperture target, moveable source method, over a wide range of E_0 and θ values. Overall agreement between theory and experiment is good at between 3 eV ≤ E_0 ≤ 15eV, which is typical of SMC calculations. The differential cross sections at around 10 eV, where pentane displays a broad structure in the integral cross section, has a typical *f*-wave oscillatory behavior, which has already been observed in n-alkanes, alcohols and amines with linear chains. In addition we notice that (discounting the very early DCSs of Fink *et al.* [51] which very likely suffer from normalization effects) the magnitude of pentane DCSs are slightly higher, while their angular dependence is similar, when compared to experimental data reported for shorter linear n-alkanes in a wide E_0 range between 1eV to 100eV.

5. Acknowledgements.

K.F. acknowledges the Fulbright Program for a fellowship to conduct this work at California State University Fullerton. M.A.K. and L.R.H. acknowledge support from National Science Foundation research grants NSF-RUI-AMO 1306742 and 0968874. A.S.B. acknowledges support from Brazilian Agency Coordenação de Aperfeiçoamento de Pessoal de Nível Superior (CAPES). M.H.F.B. acknowledges support from Brazilian agencies Conselho Nacional de Desenvolvimento Científico e Tecnológico (CNPq), and FINEP (under project CTInfra). A.S.B. and M.H.F.B also acknowledge computational support from Professor Carlos M. de Carvalho at LFTC-DFis-UFPR and at LCPAD-UFPR, and from CENAPAD-SP. We acknowledge Drs. Vincent McKoy and Carl Winstead for fruitful discussions and for useful input regarding this manuscript.

6. References.

[1] R. Minetti, M. Ribaucour, M. Carlier, C. Fittschen C and L. R. Sochet, 1994 Combust. Flame **96**, 201 (1994).

[2] S. Kojima, 1994 Combust. Flame **99**, 87 (1994).

[3] C. Q. Jiao, C. A. DeJoseph Jr and A. Garscadden, J. Phys. D: Appl. Phys. **40**, 409 (2007).

[4] S. Bhattacharjee, S. Paul, and S. Ghosh, Physics of Plasmas **21**, 082103 (2014).

[5] H. Cho, Y. S. Park, E. A. y Castro, G. L. Souza, I. Iga, L. E. Machado, L. M. Brescansin and M-T. Lee, J. Phys. B: Atom. Molec. Phys. **41**, 045203 (2008).

[6] T. Nishimura and F. A. Gianturco, J. Phys. B: At. Mol. Phys. **35**, 2873 (2002).

[7] R. Čurík, P. Čársky and M. Allan J. Phys. B: At. Mol. Opt. Phys. **41** 115203 (2008).

[8] M. H. F. Bettega, R. F. da Costa and M. A. P. Lima, Brazilian J. of Physics, **39**, 69 (2009).

[9] P. Rawat, M. G. P. Homem, R. T. Sugohara, I. P. Sanches, I. Iga, G. L. C. de Souza, A. S. dos Santos, R. R. Lucchese, L. E. Machado, L. M. Brescansin and M-T. Lee, J. Phys. B: At. Mol. Opt. Phys. **43**, 225202 (2010).

[10] L. Boesten, M. A. Dillon, H. Tanaka, M. Kimura and H. Sato, J. Phys. B **27**, 1845 (1994).

[11] D. B. Popović, D. E. David and J. Michl, and P. Čurík and P. Čársky, J. Chem. Phys. **121**, 10551 (2004).

[12] G. L. C. de Souza, M-T. Lee, I. P. Sanches, P. Rawat, I. Iga, A. S. dos Santos, L. E. Machado, R. T. Sugohara, L. M. Brescansin, M. G. P. Homem, and R. R. Lucchese, Phys. Rev. A **82**, 012709 (2010).

[13] I. P. Sanches, R. T. Sugohara, L. Rosani, M-T. Lee and I. Iga, J. Phys. B: At. Mol. Opt. Phys. **41**, 185202 (2008).

[14] G. R. Freeman, I. György, Sam S.-S Huang, Canad. J. Chem. **57**, 2626 (1979).

[15] M. Kimura, O. Sueoka, A. Hamada and Y. Itikawa, Adv. Chem. Phys. **111**, 537 (2000).

[16] M. A. Floriano, N. Gee, and G. R. Freeman J. Chem. Phys. **84**, 12 (1986).

[17] B. Boudaïffa, P. Cloutier, D. Hunting, M. A. Huels and L. Sanche, Science, **287**, 1658 (2000).

[18] M. A. Khakoo, C. E. Beckmann, S. Trajmar and G. Csanak, Phys. Rev. A **27**, 3159 (1994).

[19] K. Takatsuka and V. McKoy, Phys. Rev. A 24, 2473 (1981), Phys. Rev. A **30**, 1734 (1984).

[20] M. A. P. Lima, L. M. Brescansin, A. J. R. da Silva, C. Winstead, and V. McKoy, Phys. Rev. A 41, 327 (1990).

[21] M. H. F. Bettega, L. G. Ferreira, and M. A. P. Lima, Phys. Rev. A **47**, 1111 (1993).

[22] J. C. Traeger, C. E. Hudson and D. J. McAdoo, J. Am. Soc. Mass Spectrom. **7**, 73 (1996).

[23] ARi Industries Inc., Addison, IL 60101 USA, 1HN040B-16.3 biaxial cable.

[24] ETP Equipe Thermodynamique et Plasmas (ETP) model AF151.

[25] J. H. Brunt, G. C. King, and F. H. Read, J. Phys. B: At. Mol. Phys. **10**, 1289 (1977).

[26] M. A. Khakoo, J. Muse, H. Silva, M. C. A. Lopes, C. Winstead, V. McKoy, E. M. de Oliveira, R. F. da Costa, M. T. do N. Varella, M. H. F. Bettega, and M. A. P. Lima, Phys. Rev. A **78**, 062714 (2008).

[27] M. Hughes, K. E. James, Jr., J. G. Childers, and M. A. Khakoo, Meas. Sci. Technol. **14**, 841 (1994).

[28] R. K. Nesbet, Phys. Rev. A **20**, 58 (1979).

[29] D. F. Register, S.Trajmar, and S. K. Srivastava, Phys. Rev. A **21**, 1134 (1980).

[30] K. Fedus, C. Navarro, L. R. Hargreaves, M. A. Khakoo, F. M. Silva, M. H. F. Bettega, C. Winstead, and V. McKoy, Phys. Rev. A **90**, 032708 (2014).

[31] M. W. Schmidt, K. K. Baldridge, J. A. Boatz, S. T. Elbert, M. S. Gordon, J. H. Jensen, S. Koseki, N. Matsunaga, K. A. Nguyen, S. J. Su, T. L. Windus, M. Dupuis, and J. A. Montgomery, J. Comput. Chem. **14**, 1347 (1993).

[32] G. B. Bachelet, D. R. Hamann, and M. Schlüter, Phys. Rev. B **26**, 4199 (1982).

[33] M. H. F. Bettega, A. P. P. Natalense, M. A. P. Lima, and L. G. Ferreira, Int. J. Quantum Chem. **60**, 821 (1996).

[34] M. A. Khakoo, J. Blumer, K. Keane, C. Campbell, H. Silva, M. C. A. Lopes, C. Winstead, V. McKoy, R. F. da Costa, L. G. Ferreira, M. A. P. Lima, M. H. F. Bettega, Phys. Rev. A. **77**, 042705 (2008).

[35] M. A. Khakoo, J. Muse, H. Silva, M. C. A. Lopes, C. Winstead, V. McKoy, R. F. da Costa M. T. do N. Varella, M. H. F. Bettega, M. A. P. Lima, Phys. Rev. A **78**, 062714 (2008).

[36] T. H. Dunning, Jr., J. Chem. Phys. **53**, 2823 (1970).

[37] C. W. Bauschlicher Jr., J. Chem. Phys. **72**, 880 (1980).

[38] E. M. de Oliveira, M. T. do N. Varella, M. H. F. Bettega and M. A. P. Lima, Eur. Phys. J. D **68**, 65 (2014).

[39] R. F. da Costa, M. H. F. Bettega, M. A. P. Lima, M. C. A. Lopes, L. R. Hargreaves, G. Serna and M. A. Khakoo, Phys. Rev. A **85**, 062706 (2012).

[40] NIST Computational Chemistry Comparison and Benchmark Database, NIST Standard Reference Database Number 101, Release 16a, August 2013, Editor: Russell D. Johnson III http://cccbdb.nist.gov/ http://cccbdb.nist.gov/polcalccomp2.asp?method=3&basis=4

[41] R. Merz and F. Linder J. Phys. B **36**, 2921 (2003).

[42] W. Sohn, K. Jung and H. Ehrhardt, J. Phys. B **16**, 891 (1983).

[43] R. F. da Costa, M. H. F. Bettega, M. T. do N. Varella, E. M. de Oliveira e M. A. P. Lima, Phys. Rev. A. **90**, 052707 (2014).

[44] M. H. F. Bettega, R. F. da Costa and M. A. P. Lima, Phys. Rev. A **77**, 052706 (2008).

[45] A. R. Lopes, M. H. F. Bettega, M. A. P. Lima and L. G. Ferreira, J. Phys. B **37**, 997 (2004).

[46] M. H. F. Bettega, M. A. P. Lima and L. G. Ferreira, J. Phys. B **40**, 3015 (2007).

[46] K. Fedus, C. Navarro, L. R. Hargreaves, M. A. Khakoo, F. M. Silva, M. H. F. Bettega, C. Winstead, and V. McKoy, Phys. Rev. A **90**, 032708 (2014).

[47] H . Tanaka, L. Boesten, D. Matsunaga and T. Kudo J. Phys. B **21**, 1255 (1988).

[48] B. Mapstone and W. R. Newell J. Phys. B **25**, 491 (1992).

[49] P. J. Curry, W R Newell and A. C. H. Smith J. Phys. B **18**, 2303 (1985).

[50] R. Merz and F. Linder, J. Phys. B **31**, 4663 (1998).

[51] M. Fink, K. Jost and D. Hermann, J. Chem. Phys. **63**, 1985 (1975).

Tables.

Angle (deg)	1eV	Error	1.5eV	E_0 (eV) Error	2eV	Error	3eV	Error	5eV	Error
15									25.6	2.1
20							7.01	0.64	16.1	1.3
25			6.54	0.53	2.74	0.29	4.55	0.41	10.3	0.9
30	1.59	0.14	3.69	0.29	1.83	0.15	2.99	0.25	6.38	0.52
40	1.38	0.16	1.49	0.12	1.56	0.17	2.30	0.20	3.78	0.31
50	1.71	0.15	1.29	0.10	2.02	0.18	2.53	0.22	3.62	0.30
60	2.14	0.20	1.81	0.14	2.21	0.19	2.59	0.21	3.38	0.28
70	2.80	0.25	2.20	0.17	2.18	0.21	2.50	0.22	3.08	0.27
80	2.93	0.26	2.23	0.17	2.19	0.21	2.15	0.18	2.51	0.24
90	3.20	0.27	2.40	0.19	1.85	0.17	1.79	0.15	1.94	0.17
100	3.66	0.35	2.07	0.16	1.44	0.13	1.44	0.12	1.73	0.15
110	4.26	0.38	1.91	0.15	1.32	0.13	1.27	0.10	1.77	0.15
120	5.00	0.60	2.20	0.19	1.23	0.11	1.24	0.11	1.95	0.16
125			3.83	0.34			1.27	0.12		
129			4.65	0.83						
130	5.49	0.53			1.16	0.12	1.40	0.14	2.21	0.18
ICS	44.5	4.44	37.7	9.0	22.5	2.4	30.0	4.5	46.8	5.2
MTCS	54.8	5.1	36.3	9.9	18.4	2.2	24.7	4.8	30.8	3.4

Angle (deg)	10eV	Error	15eV	Error	20eV	E_0 (eV) Error	30eV	Error	50eV	Error	100eV	Error
5											113	10
10	45.1	4.3			69.5	5.9	78.0	6.7	66.5	5.6	25.4	2.2
15	26.8	2.3	27.4	2.8	35.3	3.1	28.8	2.4	19.7	1.7	6.84	0.59
20	17.0	1.5	16.2	1.4	17.6	1.5	12.3	1.0	6.78	0.58	2.76	0.24
25	10.5	0.9	9.84	0.85	8.54	0.70	6.25	0.53	3.30	0.28	1.87	0.19
30	6.79	0.61	6.44	0.57	5.68	0.47	4.01	0.34	2.05	0.18	1.32	0.11
40	4.15	0.36	4.18	0.37	3.27	0.27	2.25	0.19	1.38	0.12	0.597	0.052
50	3.48	0.29	2.92	0.25	2.25	0.19	1.67	0.14	0.854	0.072	0.414	0.045
60	2.82	0.22	2.14	0.19	1.72	0.14	1.14	0.09	0.455	0.053	0.311	0.027
70	2.28	0.19	1.71	0.14	1.29	0.13	0.739	0.064	0.407	0.040	0.157	0.013
80	1.79	0.16	1.42	0.12	0.98	0.10	0.563	0.047	0.319	0.028	0.104	0.012
90	1.63	0.13	1.26	0.12	0.81	0.07	0.521	0.045	0.231	0.021	0.102	0.010
100	1.79	0.15	1.26	0.12	0.91	0.08	0.511	0.050	0.204	0.021	0.148	0.022
110	2.01	0.17	1.36	0.13	0.91	0.08	0.548	0.048	0.215	0.020	0.147	0.024
120	2.16	0.19	1.40	0.12	1.05	0.09	0.670	0.059	0.306	0.036	0.156	0.016
125	2.43	0.24										
129												
130			1.56	0.15	1.11	0.09	0.768	0.076	0.412	0.042	0.201	0.023
ICS	46.3	4.3	39.6	5.2	39.4	4.1	33.9	4.9	23.7	4.5	13.7	1.8
MTCS	27.7	2.5	22.3	2.9	14.4	1.4	10.1	1.0	5.61	0.863	3.01	0.605

Table I: Experimental DCSs (10^{-16}cm^2/sr), ICSs and MTCs (10^{-16}cm^2) for elastic electron scattering from pentane. Error bars (1 standard deviation) include uncertainties in helium elastic DCSs (5-8%), uncertainties in flow-rates (3-5%), statistical uncertainties (1-5%) and standard deviation uncertainties of multiple DCSs measurements.

Figures.

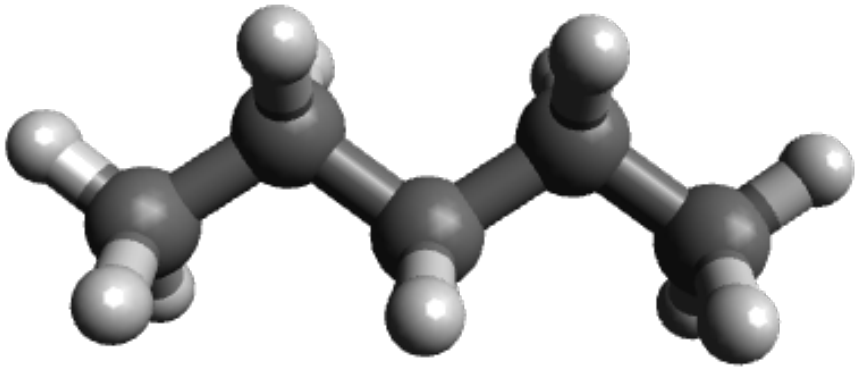

Fig. 1 (color online): Stick and ball model of pentane (C_5H_{12}).

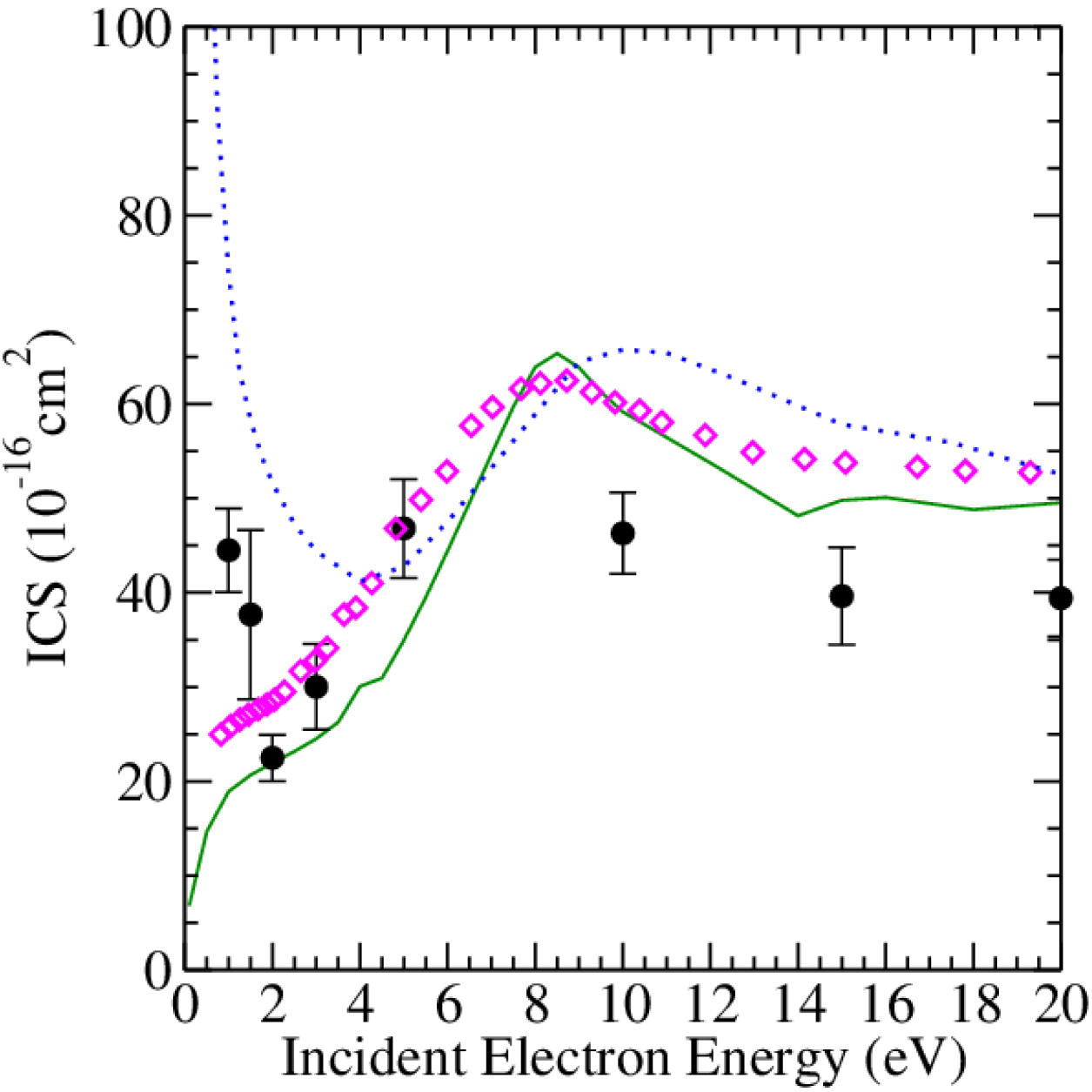

Fig. 2 (color online): Integral Cross Section (ICS) for elastic scattering of electrons by pentane, in the static exchange-polarization approximation (—) and experimental elastic ICS (•) for pentane. We compare our results with experimental total cross section (TCS) (◊) from [15] and calculated data for n-pentanol (···) obtained with the SMCPP method [38].

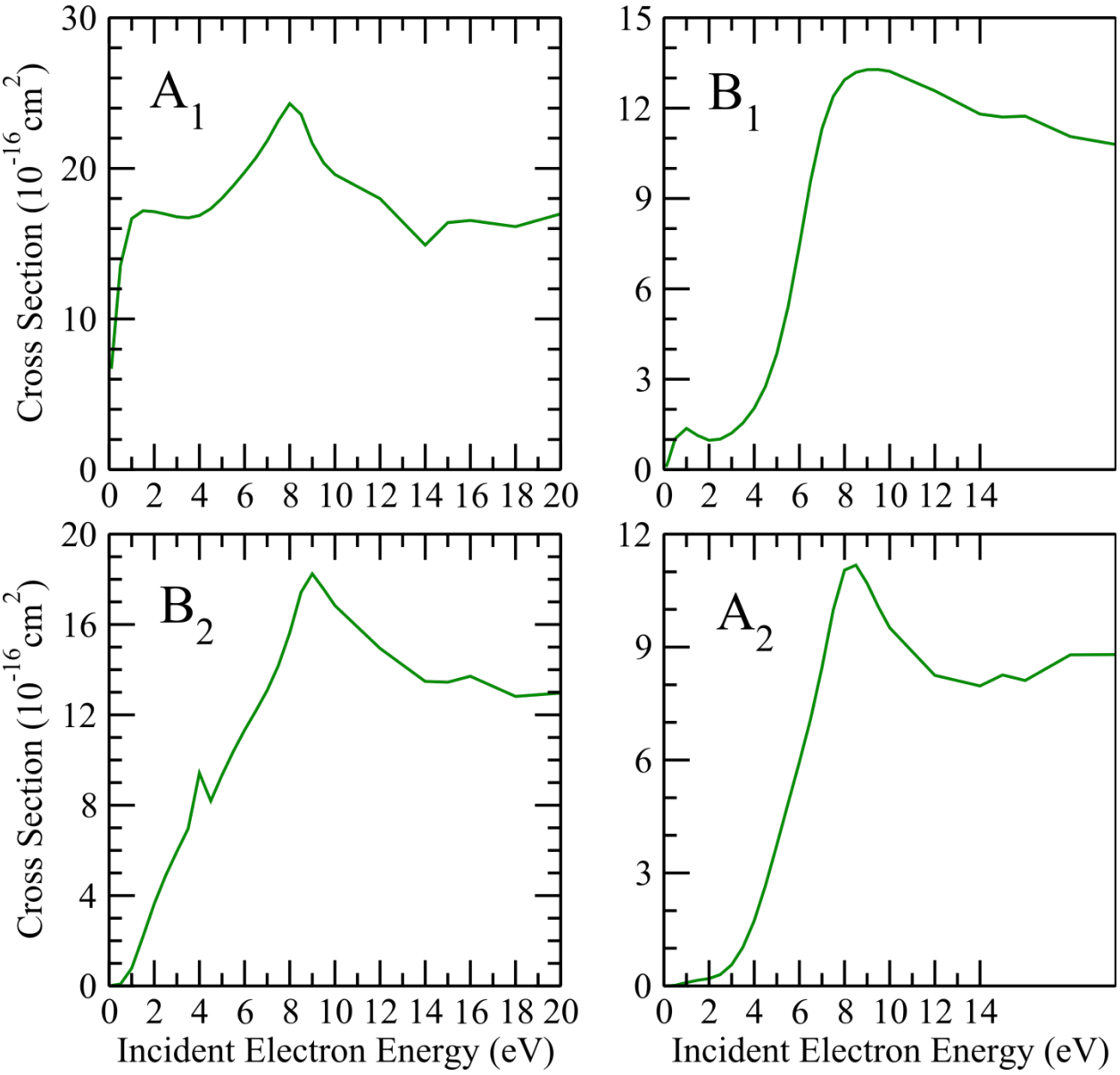

Fig. 3 (color online): Symmetry decomposition according to the C_{2v} point group of the ICS for elastic scattering of electrons by pentane. See text.

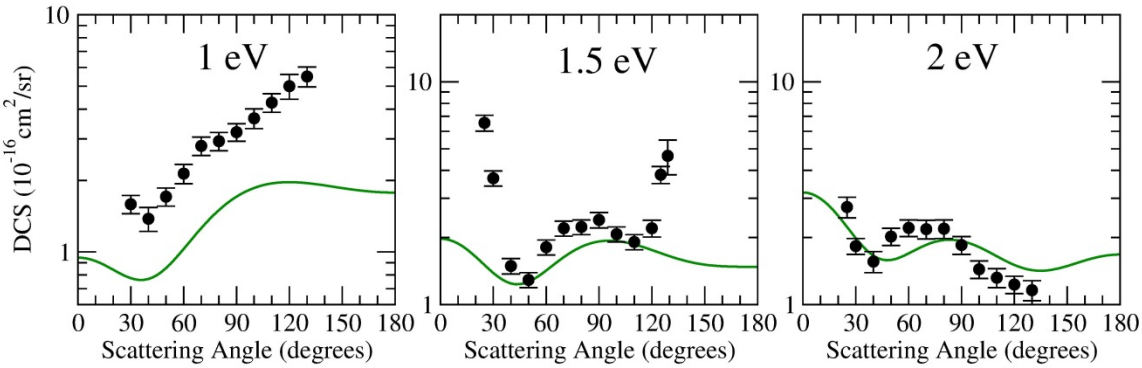

Fig. 4 (color online): Differential cross sections for elastic scattering of electrons by pentane at 1, 1.5, and 2 eV. We present results in the SEP approximation and compare with the experimental data for pentane. Legend is the same as in Fig. 2.

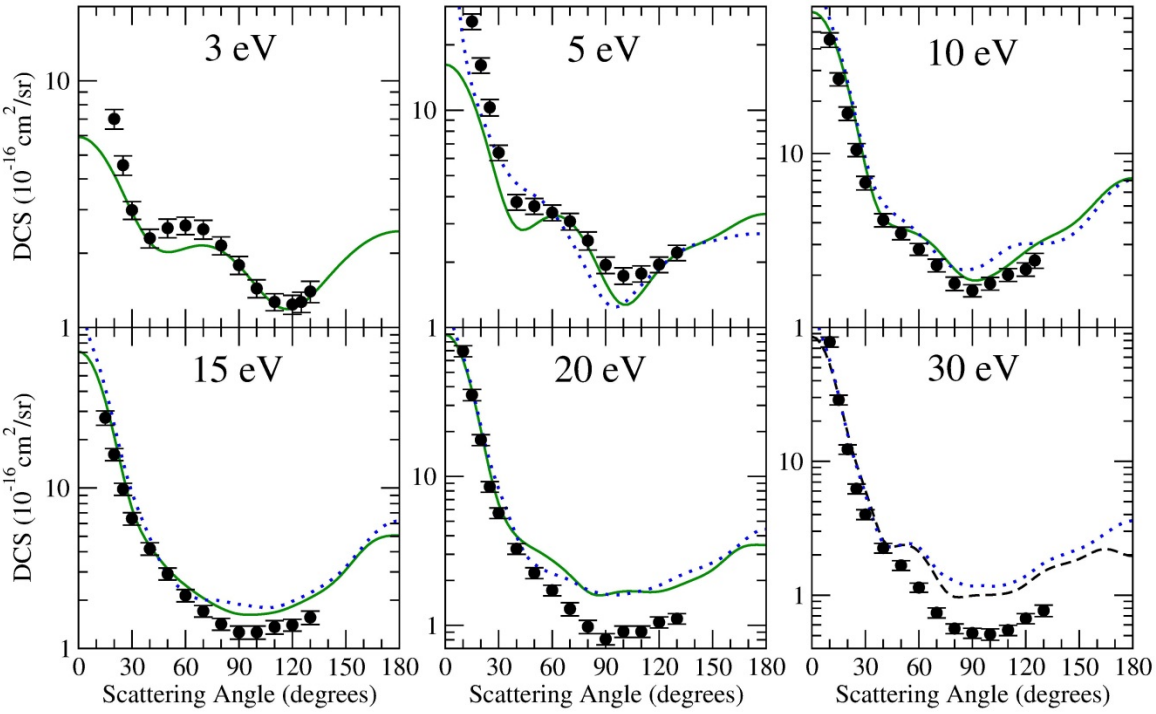

Fig. 5 (color online): Differential cross sections for elastic scattering of electrons by pentane at 3, 5, 10, 15, 20 and 30 eV. We present results in SEP approximation. We compare our DCS with calculated DCS for n-pentanol [38]. Legend is the same as Fig. 2.

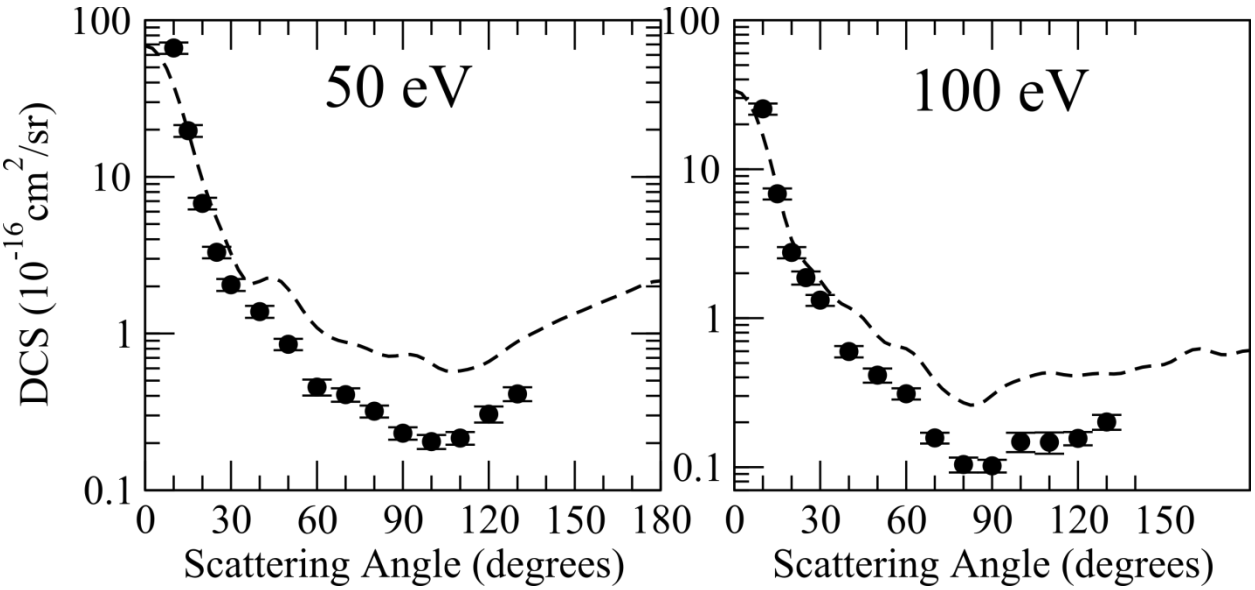

Fig. 6 : Differential cross sections for elastic scattering of electrons by pentane at 50 and 100 eV. We present results in the SE (- - - -) approximation and compare with present experimental data (•).

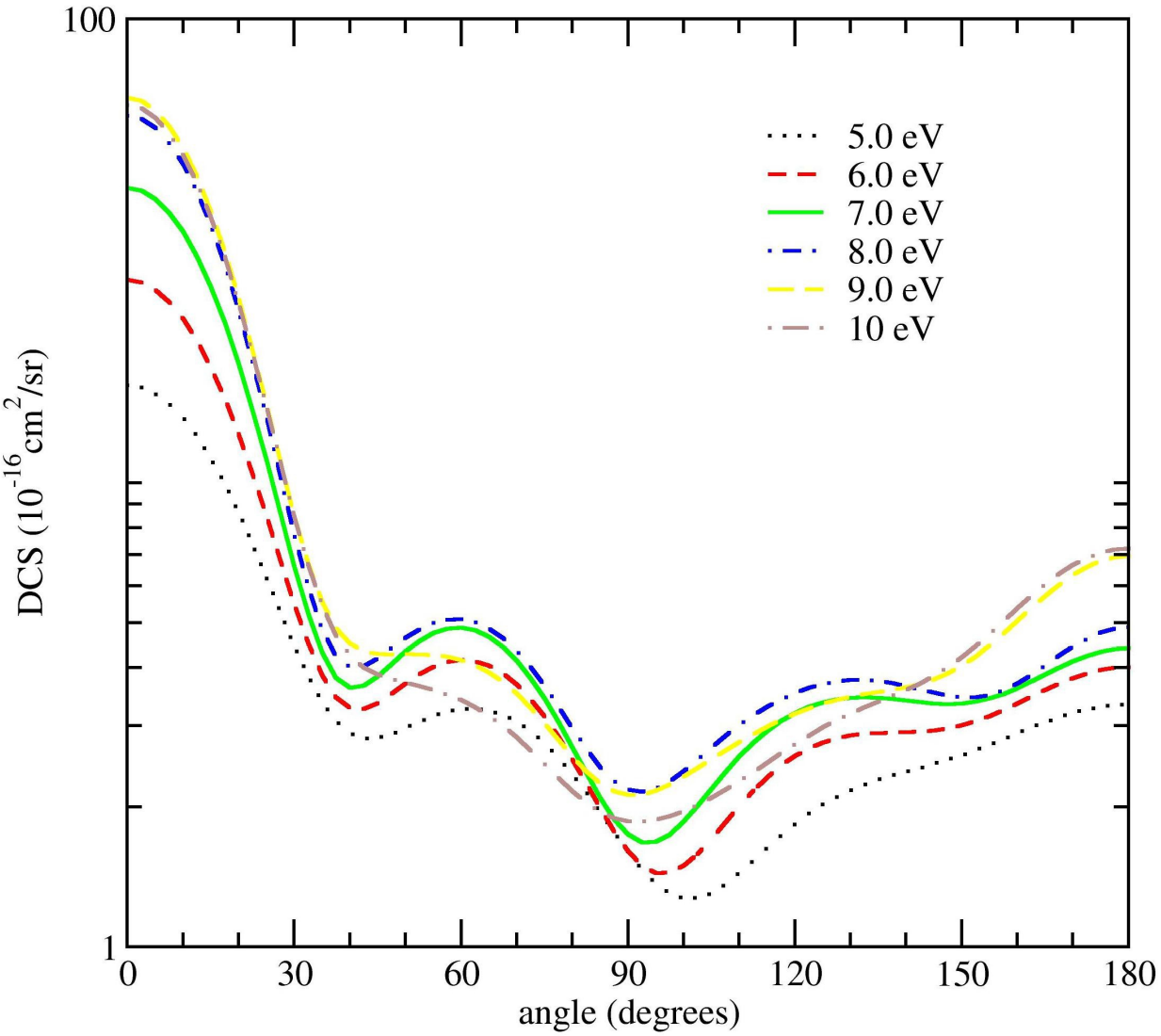

Fig. 7 (color online): Differential cross sections for elastic scattering of electrons by pentane from 5eV to 10eV showing the *f*-wave distributions at these energies.

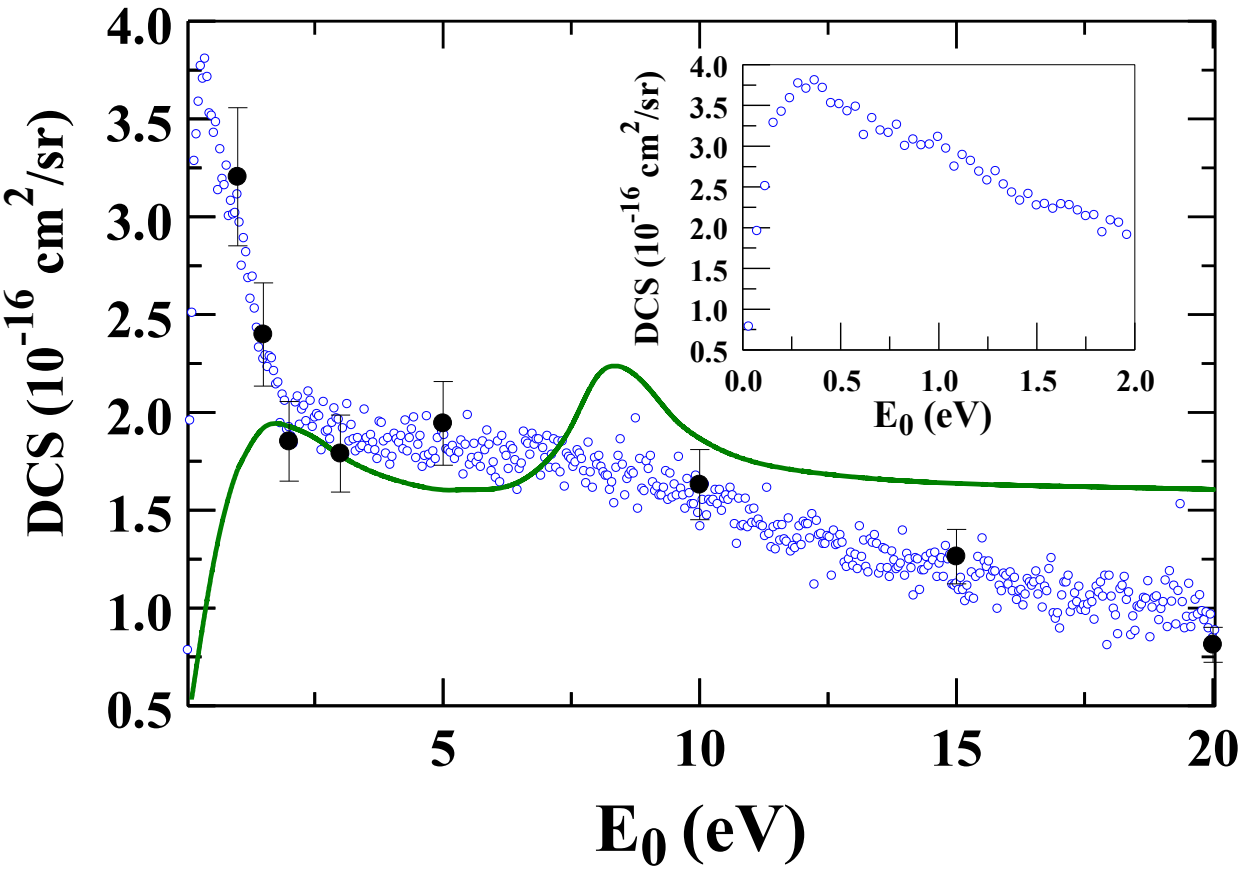

Fig. 8 (color online): Differential cross sections for elastic scattering of electrons by pentane at $\theta=90^o$ as a function of E_0. Legend: O: Experiment at $\theta=90^o$ as a function of E_0; — SEP DCSs; • normalized experimental DCSs at $\theta=90^o$ from Table 1. The inset shows the experimental DCSs for $E_0 \leq 2$eV. See text.

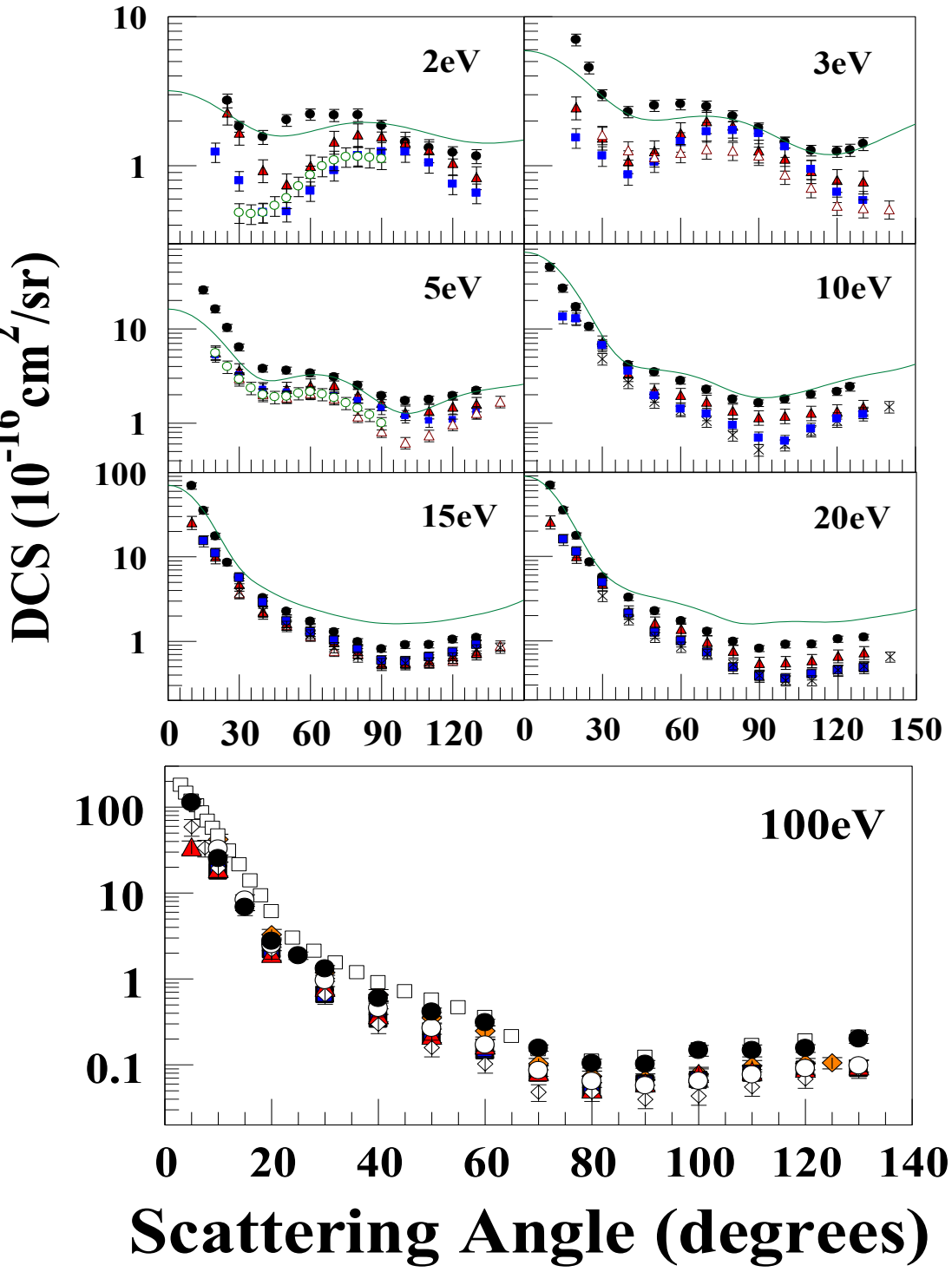

Fig. 9 (color online): DCSs for elastic scattering of electrons by ethane, propane, butane and pentane for selected E_0 values. Legend: **Ethane:** ■, Tanaka *et al.* [47]; Δ Mapstone and Newell [48], Curry and Newell [49], O Merz and Linder [50], ◊ Rawat *et al.* [9] and □ Fink *et al.* [51]. **Propane:** ▲, Boesten *et al.* [10] and ♦ Souza *et al.* [12]. **Butane:** O Sanches *et al.* [13]. **Pentane:** • Present experiment and — present calculations. See text for discussion.